

# Correlated emission of electron-current waves

Shane P. Kelly, Eric Kleinherbers, Yanyan Zhu, and Yaroslav Tserkovnyak

*Department of Physics and Astronomy and Mani L. Bhaumik Institute for Theoretical Physics,  
University of California at Los Angeles, CA 90095*

Correlated emission of light offer a potential avenue for entanglement generation between atomic spins, with potential application for sensing and quantum memory. In this work, we investigate the conditions for the correlated emission by color centers into an electronic bath of conduction electrons. Unlike emission into bosonic modes, electrons can absorb energy via two-particle processes across a large range of length scales. We find that two length scales are particularly relevant: one set by the Fermi velocity and the frequency of the color centers  $v_F/\Delta$ , and the other set by the Fermi wavelength  $\lambda_F \ll v_F/\Delta$ . Subradiance requires emitters to be spaced at a distance closer than the Fermi wavelength, while superradiance requires spacing less than  $\sqrt{\lambda_F v_F}/\Delta$ , so long as the emitters are initialized with coherence. We show that the emitted current burst has a spiral form, and we discuss the experimental possibility to observe correlated dissipation by color-center qubits coupled to electronic environments.

Correlated emission occurs when a collection of localized quantum systems emit energy coherently into an environment. First identified by R. H. Dicke [1], the phenomenon has been observed in platforms ranging from cold atomic gases [2–4], superconducting circuits [5], photonic waveguides [6, 7] and nitrogen-vacancy centers (NVs) in diamond [8–10]. It is important for quantum technologies, both as a potential hazard for error correction [11], and as a resource for entanglement generation [12] and quantum memories [13].

Numerous investigations have considered a collection of qubits coupled to photonic environments [14], and recently theoretical work has considered the coupling of qubits to a magnonic environment [15]. While independent emission is generic, correlated emission occurs only if the emitters are spaced closer than the wavelength of the emitted bosonic excitation. When that is the case, two types of correlated emission are generally identified: subradiance, when the rate of emission is suppressed due to cooperative effects, and superradiance, when the rate of emission is cooperatively enhanced.

In contrast, correlated emission into a fermionic environment has, to our knowledge, not been considered so far. Nonetheless, recent experiments [16, 17] have observed the dissipative coupling of color centers, such as the NV center, to the magnetic noise produced by conduction electrons. In these experiments, single qubits are used as magnetic-field sensors [18–21] of a condensed-matter environment. When multiple qubits are available, the condensed-matter environment has the possibility to mediate cooperative effects through dissipation, such as correlated emission.

A similar cooperative, yet coherent effect, occurs when conduction electrons mediate long-range exchange interactions [22–24] between localized spins. These coherent interactions may result in spin-glass physics [25], characterized by disordered ground states and slow relaxation. In comparison, color centers are placed outside the electron gas and can be optically controlled and

read out, allowing access to far-from-equilibrium quantum states [26], microscopic probes of spin dynamics, and the tunable weak-coupling regimes relevant for correlated emission [1, 12, 14].

Thus, we theoretically consider the possibility of collective emission into an electronic environment. The primary challenge is that, unlike a bosonic environment such as the electromagnetic vacuum, noise from an electronic gas occurs within a large range of length scales for a fixed emitter frequency. Electronic noise from conduction electrons is generically captured by the two-particle spectrum of a Fermi gas (see Fig. 1) and is characterized by two length scales: the Fermi wavelength  $\lambda_F$  and a length  $v_F/\Delta$  depending on the frequency of the emitter  $\Delta$  and the Fermi velocity  $v_F$ .

The main result of this work is the emitter spacing at which subradiance and superradiance will occur due to a two-dimensional electron gas: Subradiance requires emitters to be spaced closer than the Fermi wavelength, while the requirement for superradiance is generically looser.

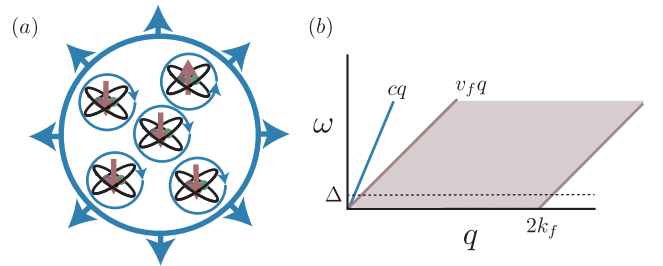


FIG. 1. (a) Schematic representation of the correlated emission of magnetic dipoles into an electronic bath of conduction electrons. (b) Sketch of noise spectrum for a photonic (blue) and electronic (red) bath. Photonic noise is peaked on the curve  $\omega = cq$  set by the dispersion of light. Electronic noise is characterized by the particle-hole continuum with noise having spectral weight in the red-shaded region. Qubits couple to a single frequency of the noise  $\Delta$ .

In particular, it depends on whether the emitters are initialized in a state with or without coherence between the two levels of the emitter. If the emitters are initialized without coherence, superradiance requires a spacing on a scale similar to the Fermi wavelength. While if the emitters are initialized with coherence, superradiance can occur with a spacing  $a$  significantly further than the Fermi wavelength so long as  $a < \sqrt{\lambda_F v_F / \Delta}$ .

*Bosonic vs fermionic environments.*— In general, collective emission can occur when an ensemble of localized quantum systems couple to a common  $d$ -dimensional environment of volume  $V$ . As a concrete example, we will focus on spin-half magnetic dipoles, leaving the straightforward generalization to arbitrary two-level systems implicit. In their ground state, the magnetic dipoles point in the  $-\hat{z}$  direction. The magnetic dipoles are described by the Pauli spin operators  $\boldsymbol{\sigma}_n = (\sigma_n^x, \sigma_n^y, \sigma_n^z)$ , and we model their evolution using the Hamiltonian

$$H = \frac{\hbar\Delta}{2} \sum_n \sigma_n^z + \frac{\hbar\gamma_e}{2} \sum_n \mathbf{B}(\mathbf{r}_n) \cdot \boldsymbol{\sigma}_n + H_E, \quad (1)$$

where  $\hbar\Delta$  is the energy spacing between the two levels of the magnetic dipole,  $\mathbf{B}(\mathbf{r}_n)$  is the environment-induced magnetic-field operator at the position of the  $n$ th dipole,  $H_E$  is the Hamiltonian of the environment creating the magnetic fields, and  $-\gamma_e$  is the gyromagnetic ratio of the magnetic dipole. Below, we assume the environment is translationally invariant.

Under a Markovian weak-coupling approximation, the dynamics of magnetic dipoles are described by a Lindblad master equation containing both coherent mediated interactions and dissipative processes such as excitation, dephasing, and decay. We consider an environment at zero temperature, such that excitation processes are suppressed. Furthermore, we neglect dephasing and the coherent mediated interactions so that we can directly identify when nonlocal decay may qualitatively affect the relaxation dynamics. The resulting Lindblad equation in the rotating frame of the dipoles is

$$\partial_t \rho = \sum_{nm} \gamma_{nm} \left( \sigma_n^- \rho \sigma_m^+ - \frac{1}{2} \{ \sigma_m^+ \sigma_n^-, \rho \} \right), \quad (2)$$

where  $\sigma_n^\pm = (\sigma_n^x \pm i\sigma_n^y)/2$  are the Pauli raising and lowering operators, and the nonlocal decay rates are determined by the magnetic field noise  $\gamma_{nm} = \gamma(\mathbf{r}_n - \mathbf{r}_m) = \frac{\gamma_e^2}{4} C^{-+}(\Delta, \mathbf{r}_n - \mathbf{r}_m)$  at resonant frequency  $\Delta$ . The magnetic-field noise at arbitrary frequency  $\omega$  is described by the correlation function

$$C^{-+}(\omega, \mathbf{r}_n - \mathbf{r}_m) = \int_{-\infty}^{\infty} dt e^{i\omega t} \langle B^-(t, \mathbf{r}_n) B^+(0, \mathbf{r}_m) \rangle$$

between the two circular polarizations of the magnetic field  $B^\pm = B^x \pm iB^y$ .

First, we consider a bosonic environment described by a collection of bosonic modes  $b_{\mathbf{q}}$  with dispersion  $\omega_{\mathbf{q}}$  and

governed by the Hamiltonian  $H_E = \sum_{\mathbf{q}} \hbar\omega_{\mathbf{q}} b_{\mathbf{q}}^\dagger b_{\mathbf{q}}$ . The magnetic fields are linearly related to the bosonic creation and annihilation operators by

$$\mathbf{B}(\mathbf{r}) = \sum_{\mathbf{q}} \frac{e^{i\mathbf{q}\cdot\mathbf{r}}}{\sqrt{V}} \mathbf{g}_{\mathbf{q}} b_{\mathbf{q}} + H.c., \quad (3)$$

such that the magnetic dipoles decay via emission of a boson. Bosons can only be created at a momentum  $\mathbf{q}$  determined by their energy  $\hbar\omega = \hbar\omega_{\mathbf{q}}$ . Accordingly, the magnetic-field noise is constrained as  $C^{-+}(\omega, \mathbf{q}) \propto \delta(\omega_{\mathbf{q}} - \omega)$ , see Fig. 1, where  $C^{-+}(\omega, \mathbf{q}) = \int d^d \mathbf{r} e^{-i\mathbf{q}\cdot\mathbf{r}} C^{-+}(\omega, \mathbf{r})$ .

In contrast, an environment of fermionic particles necessarily couples via particle scattering: the magnetic-field operator is a bosonic operator and must be expanded as a product of an even number of fermion operators. We consider a noninteracting electron gas described by the Hamiltonian  $H_E = \sum_{\mathbf{k}} \hbar\omega_{\mathbf{k}} f_{\mathbf{k}}^\dagger f_{\mathbf{k}}$ , where  $f_{\mathbf{k}}$  is the fermion annihilation operator at wave vector  $\mathbf{k}$  and  $\omega_{\mathbf{k}}$  is now the electron dispersion. In a magnetostatic approximation, the magnetic fields are linearly related to the electron spin and current densities. Thus, the magnetic-field operators have, in a homogeneous environment, the form

$$\mathbf{B}(\mathbf{r}) = \sum_{\mathbf{k}, \mathbf{q}} \frac{e^{i\mathbf{q}\cdot\mathbf{r}}}{V} \mathbf{V}_{\mathbf{k}, \mathbf{k}+\mathbf{q}} f_{\mathbf{k}}^\dagger f_{\mathbf{k}+\mathbf{q}}, \quad (4)$$

where the matrix elements  $\mathbf{V}_{\mathbf{k}, \mathbf{k}+\mathbf{q}}$  are determined by the geometry of the magnetostatic problem, and we have omitted the spin indices. Physically, the magnetic-dipole coupling  $\propto \boldsymbol{\sigma}_n \cdot \mathbf{B}$  describes processes in which energy is exchanged between the  $n$ th magnetic dipole and a bosonic electron-hole pair with momenta  $\mathbf{k} + \mathbf{q}$  and  $\mathbf{k}$ .

The kinetics of this process determine the magnetic field noise governing correlated emission. The magnetic-field noise at thermal equilibrium takes the form

$$C^{-+}(\omega, \mathbf{q}) = \int \frac{d^d \mathbf{k}}{(2\pi)^{d-1}} V_{\mathbf{k}, \mathbf{k}+\mathbf{q}}^- V_{\mathbf{k}+\mathbf{q}, \mathbf{k}}^+ n_{\mathbf{k}} (1 - n_{\mathbf{k}+\mathbf{q}}) \times \delta(\omega + \omega_{\mathbf{k}} - \omega_{\mathbf{k}+\mathbf{q}}),$$

determined by the matrix elements  $V_{\mathbf{k}, \mathbf{k}+\mathbf{q}}^\pm = V_{\mathbf{k}, \mathbf{k}+\mathbf{q}}^x \pm iV_{\mathbf{k}, \mathbf{k}+\mathbf{q}}^y$ , the Fermi-Dirac occupation function  $n_{\mathbf{k}}$ , and the kinetic constraint  $\delta(\omega + \omega_{\mathbf{k}} - \omega_{\mathbf{k}+\mathbf{q}})$  which restricts the particle at wave vector  $\mathbf{k}$  to absorb only momentum  $\hbar\mathbf{q}$  and energy  $\hbar\omega$ . At low temperature, and small energy transfer  $\hbar\omega \ll E_F$ , the magnetic-field noise arises from electron dynamics near the Fermi surface. The frequencies and wave vectors at which noise can occur are shown in Fig. 1. The largest possible wave vector  $\mathbf{q}$ , for small  $\hbar\omega$ , has magnitude  $2k_F$  and is due to an electron scattering between antipodal points on the Fermi surface [27]. The smallest wave vector has magnitude  $\omega/v_F$ .

We now consider a random distribution of dipoles with mean spacing  $a$ , at a fixed height  $d$  above a two-dimensional conductor. This configuration is characteristic of the experiments in Refs. [16, 17, 28] probing the

dynamics of a single NV [29] at a fixed height above a conductor. In this setting, the NV predominantly couples to transverse current waves [30–32]: longitudinal waves occupy a negligible region of phase space and are suppressed by the Coulomb interaction. The coupling-matrix elements between the transverse currents and NVs are determined in the Supplemental Material [33] and are

$$\mathbf{V}_{\mathbf{k}, \mathbf{k}+\mathbf{q}}(0) = (\hat{\mathbf{q}} + i\hat{\mathbf{d}}) \frac{2\pi e\hbar}{cm} e^{-qd} (\hat{\mathbf{q}}_{\perp} \cdot \mathbf{k}), \quad (5)$$

where  $\mathbf{q}$  points in plane;  $\hat{\mathbf{d}}$  points perpendicular to the plane; and  $\hat{\mathbf{q}}_{\perp} = \hat{\mathbf{q}} \times \hat{\mathbf{d}}$  is the in-plane unit vector orthogonal to  $\mathbf{q}$ . The constants  $c$ ,  $m$ , and  $e$  are the speed of light, effective electron mass, and magnitude of the electron charge. Finally, we consider the situation in which the dipoles are aligned perpendicular to the plane  $\hat{\mathbf{z}} = \hat{\mathbf{d}}$ .

The Oersted magnetic-field noise produced by the transverse-current fluctuations [33] is shown in Fig. 2(a). This noise has spectral weight over a range of wave vectors  $q \in (\omega/v_F, 2k_F)$ . In this range, the transverse current fluctuations decay as  $1/q$ . The corresponding decay-rate matrix  $\gamma_{nm}$  is shown in Fig. 2(b) as a function of the dipole separation  $r = |\mathbf{r}_n - \mathbf{r}_m|$ . First, consider the case when the dipoles are at small height  $d < \lambda_F$ . In this limit, the decay-rate matrix remains nearly constant for dipole separations  $r < \lambda_F$ . For larger separations  $\lambda_F < r < v_F/\Delta$ , the decay-rate matrix decays as  $1/r$ , before crossing over to  $1/r^2$  for  $r > v_F/\Delta$ . When the dipoles are placed at a larger height  $d > \lambda_F$ , the decay-rate matrix stays constant over a larger separation  $r < d$ , before crossing over to a  $1/r$  decay for  $d < r < v_F/\Delta$ .

*Subradiance.*— Subradiance is the phenomenon in which the decay of the collective ensemble is slower than for independent emitters. For two dipoles, there is a slow decaying state with decay rate  $\gamma_0 - |\gamma_a| \geq 0$ , where  $\gamma_a$  is the non-local rate for two dipoles with separation  $|\mathbf{r}_n - \mathbf{r}_m| = a$ . As the separation decreases, the non-local rate approaches the local rate  $\gamma_a \rightarrow \gamma_0$ , and the singlet state becomes dark (does not decay). For noise produced by transverse-current fluctuations, this occurs when  $a \lesssim \lambda_F$ , as shown in Fig. 2(b) for  $d = 0$ . For dipoles placed further from the material  $d > \lambda_F$ , subradiance occurs for larger spacing  $a \lesssim d$ .

These conclusions for two dipoles generalize to a homogeneous collection of dipoles except for one caveat: For a homogeneous distribution of dipoles with mean spacing  $a > \lambda_F$ , there is a finite probability that two dipoles have a spacing  $r < \lambda_F$ . Thus, even at low densities, there exist subradiant states. Nonetheless, these subradiant states are statistically rare and localized at the two dipoles with atypical spacing  $r \ll a$ . Only when the densities are sufficiently large,  $n > \min(\lambda_F^{-2}, d^{-2})$ , do subradiant states become typical and relevant for collective relaxation dynamics. This is confirmed in the SM [33] via numerical diagonalization of the decay-rate matrix.

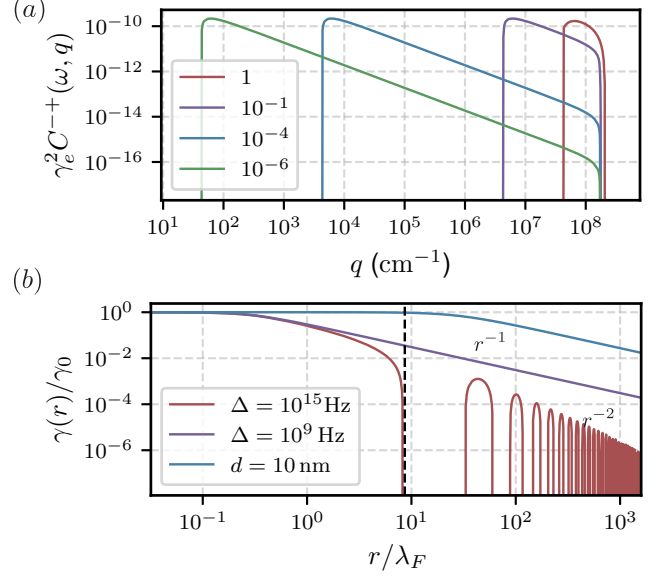


FIG. 2. (a) Magnetic-field spectral density  $\gamma_e^2 C^{+-}(q, \omega)$  in units of  $\text{Hz cm}^2$ . The legend shows  $\hbar\omega/E_F$ . The curves were evaluated using  $\gamma_e = 2.8 \text{ MHz/G}$  for the gyromagnetic ratio [28] and  $d = 0$  for the height. (b) Space dependence of the decay-rate matrix  $\gamma_{nm} = \gamma(\mathbf{r}_n - \mathbf{r}_m)$ . For the red and purple line, the height is  $d \approx 0$ , while for the blue line the frequency is  $\Delta = 1.2 \text{ GHz}$ . In both figures, we use the free electron mass  $m = 9.1 \times 10^{-28} \text{ g}$  and a Fermi velocity  $v_F = 10^8 \text{ cm/s}$  typical for an electron gas. Accordingly, the Fermi surface is defined by  $\lambda_F \approx 10^{-8} \text{ cm}$  and  $E_F/\hbar \approx 10^{16} \text{ Hz}$ . The black dashed line shows  $v_F/\Delta$  for  $\Delta = 10^{15} \text{ Hz}$ , the scale at which the red curve crosses over from  $1/r$  to an oscillatory  $1/r^2$ .

*Superradiance.*— In contrast to subradiance, superradiance can occur when the dipoles are spaced at a distance much larger than either the Fermi wavelength or the height  $d$ . Our consideration of superradiance is twofold: First, we consider the acceleration of the decay process for the dipoles prepared in their excited state. Second, we consider the decay rate for dipoles prepared in a superposition between the excited and ground state. In both situation we consider the time dependence of the collective spin  $S^z = \frac{\hbar}{2} \sum_n \langle \sigma_n^z \rangle$ , and we will be interested in the total decay rate  $R = -\partial_t S^z / \hbar$ , and its time derivative  $\partial_t R$ . In this section, we consider the limit  $d = 0$  when NVs are close to the material.

While exact simulation of the dissipative quantum dynamics of Eq. (2) is computationally prohibitive, properties of early time dynamics are easy to compute and have been used to determine conditions required for superradiance [34, 35]. First consider the situation when all dipoles are prepared in their excited state. The initial total decay rate  $R$  is always equal to the total decay rate for independent emission  $R(t=0) = N\gamma_0$  regardless of whether collective effects are present or not. Collective emission, at early times, is instead distinguished by the change in the total decay rate  $\partial_t R$ . For independent emission, the

decay process slows and  $\partial_t R(t=0) < 0$ , while for superradiance, the decay of the first excitation accelerates the decay of the second such that  $\partial_t R(t=0) > 0$ . In the case that the dipoles are closely packed and  $\gamma_{nm} = \gamma_0$ , the change in the total decay rate  $\partial_t R$  is positive and scales with  $N^2$ .

Now consider the case when the dipoles are placed in random locations spanning an area  $A$  and with a density  $n$ . In the SM [33], we show that for a homogeneous distribution of dipoles, all in the excited state, the change in the total decay rate is given by

$$\frac{\partial_t R}{N\gamma_0^2} = \pi\lambda_{\text{SR}}^2 n - 1, \quad (6)$$

where  $\lambda_{\text{SR}}$  sets the superradiance length scale at which correlated emission occurs:

$$\pi\lambda_{\text{SR}}^2 = \frac{1}{C^{--}(\Delta)^2} \int \frac{dq q}{2\pi} C^{--}(\Delta, q)^2. \quad (7)$$

Here,  $C^{--}(\Delta) = (2\pi)^{-1} \int dq q C^{--}(\Delta, q)$  is the local spectral density at a frequency  $\Delta$ , and we have assumed the noise is isotropic in  $\mathbf{q}$ .

The magnetic-field noise produced by the transverse current fluctuations allows for the approximation  $C^{--}(\Delta, q) \propto 1/q$  for  $q \in (\Delta/v_F, 2k_F)$  and 0 elsewhere, see Fig 2. In this case, the superradiance length is given by  $\lambda_{\text{SR}}^2 \approx \lambda_F^2 \ln(4E_F/\hbar\Delta)$ , where we have assumed  $\lambda_F \ll v_F/\Delta$ . Thus, a superradiant acceleration,  $\partial_t R > 0$ , requires that the density of dipoles is larger than  $n > \lambda_{\text{SR}}^{-2}/\pi \approx \lambda_F^{-2}/\ln(4E_F/\hbar\Delta)\pi$ . In comparison to subradiance, which requires dipole densities  $n \gtrsim \lambda_F^{-2}$ , superradiant acceleration occurs at lower densities, albeit by a logarithmic factor  $\ln(4E_F/\hbar\Delta)$  (about 10 for typical NV frequencies and metallic Fermi surfaces).

Nonetheless, collective effects can be observed at even lower densities if the magnetic dipoles are prepared in a state with coherence between the excited and ground state. Consider the situation, easily initialized by a  $\pi/2$  pulse, in which each dipole is in an equal superposition of the excited state and the ground states  $(|-\rangle + |+\rangle)/\sqrt{2}$ . For independent emission, the total decay rate scales linearly with the number of emitters  $R \propto N$ . While for a constant decay-rate matrix  $\gamma_{nm} = \gamma_0$ , the total decay rate scales quadratically  $R \propto N^2$ . In a generic setting, the instantaneous decay rate is given by  $R = \frac{1}{2} \sum_k \gamma_{kk} + \frac{1}{2} \sum_{n \neq m} \gamma_{nm}$ , and when the dipoles are distributed randomly in a region of radius  $\sqrt{A}$ , it is given by

$$R \approx \frac{N}{2} \gamma_0 + N\pi n \int_0^{\sqrt{A}} r dr \gamma(r), \quad (8)$$

where we have approximated the sum over dipole locations via a disorder average over their distribution [33].

For dipoles coupled to transverse current fluctuations and placed close to the sample  $d < \lambda_F$ , the decay rate

follows  $\gamma(r) \propto 1/r$  for  $r \in (\lambda_F, v_F/\Delta)$ . Thus, so long as  $\lambda_F < \sqrt{A} < v_F/\Delta$ , there is a superradiant enhancement of the total decay rate  $R \approx Nn\gamma_0\sqrt{A}\lambda_F/2$  scaling with the size of the region  $\sqrt{A}$  occupied by the dipoles. For  $\sqrt{A} > v_F/\Delta$ , the integrand in Eq. (8) becomes highly oscillatory when  $r > v_F/\Delta$ , and we estimate  $R \approx Nn\gamma_0\lambda_F v_F/\Delta$  for  $A \rightarrow \infty$ . Thus, so long as the average spacing between the dipoles is smaller than

$$\lambda'_{\text{SR}} = \sqrt{\lambda_F v_F/\Delta}, \quad (9)$$

we expect a collective enhancement of the decay process scaling with  $n\lambda_{\text{SR}}'^2$ . Note that for a quadratic dispersion,  $\lambda'_{\text{SR}}$  is the de-Broglie wavelength for an electron at energy  $\hbar\Delta$ : approximately  $1 \mu\text{m}$  for a free electron and  $\Delta \approx 1 \text{ GHz}$ . For dipoles further from the sample  $d > \lambda_F$ , the spacing must be smaller than  $\lambda'_{\text{SR}} \approx \sqrt{dv_F/\Delta}$ .

Note that, while the condition  $\partial_t R(t=0) > 0$  is sufficient for a superradiant burst, it is not known if it is necessary. Thus, we are left with an open question regarding the intermediate time dynamics for a fully-excited initial state. It is conceivable that at early times  $\partial_t R < 0$  due to a slow development of coherence, but at intermediate times, coherence could become sizable leading to superradiance. We can therefore not rule out the possibility of superradiance for a state lacking coherence between the ground and excited state and for densities  $n < k_F^2/4\pi \ln(4E_F/\hbar\Delta)$ . To resolve this possibility, an experiment or more elaborate many-body methods are required and are beyond the scope of this work.

*Emitted Currents.*— For a fermionic environment, energy is carried away by a redistribution of the particles around the Fermi surface. This redistribution forms transverse-current waves when the coupling with dipoles is the magneto-static coupling above. We determine these waves by linear response to the magnetic fields produced during the decay of the dipoles [33]. For simplicity, we consider the magnetic dipoles to be placed all at the same location. In this configuration, the collection of dipoles form a macrospin that undergoes classical Landau-Lifshitz damping [33]. In Fig. 3, we show the transverse-current waves emitted from the decaying macrospin. The static response corresponds to Landau diamagnetism (not resolved in the figure), while the dynamic response (shown in the figure) captures the radiated energy.

The features observed in Fig. 3 can be explained as follows. First, the environment is a gas of free particles, which ensures that the current distribution undergoes ballistic expansion  $J^\alpha(\boldsymbol{\rho}, t) = g^\alpha(\boldsymbol{\rho})f^\alpha(\varphi, \rho - v_F t)$ , where  $\varphi$  and  $\rho$  are the azimuthal and radial coordinates of the two-dimensional electron gas. Second, the decaying macrospin has two time scales: the first  $\propto \gamma_0^{-1}/N$  set by the decay of the total  $S^z$  and another  $\Delta^{-1}$  set by the frequency of the dipole. In the figure we considered a typical situation in which  $\Delta > N\gamma_0$ , and plot the azimuthal component of the current distribution. Due to



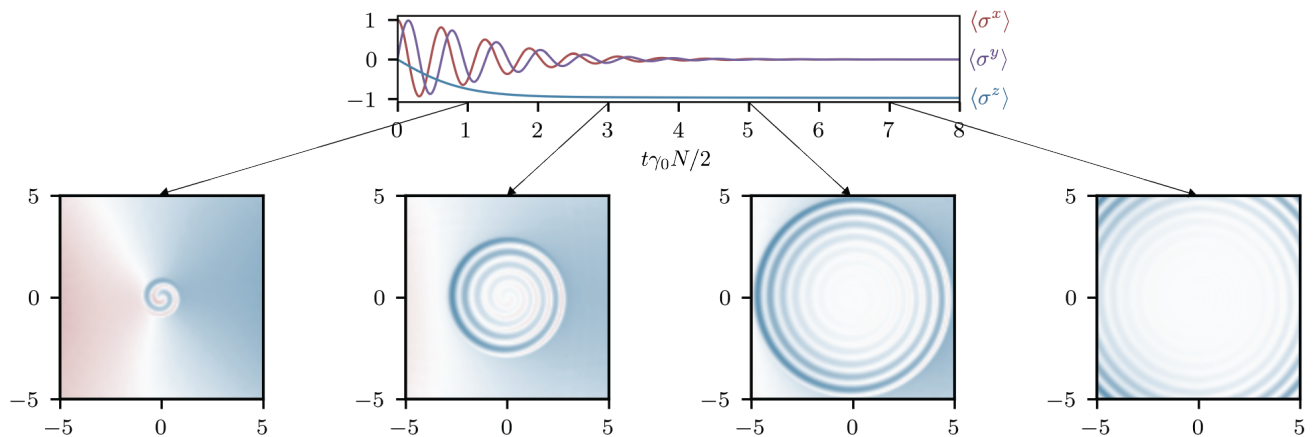


FIG. 3. Dynamics of the macrospin  $\langle \sigma \rangle = 2 \langle \mathbf{S} \rangle / \hbar N$  and the rescaled azimuthal component of the far-field emitted current distribution  $\rho \hat{\phi} \cdot \mathbf{J}(\rho, t)$ : Blue corresponds to clockwise current flow, while red corresponds to counterclockwise current flow. The  $x$  and  $y$  axes have units of  $2v_F/\gamma_0 N$ . For illustrative purposes, the figure shows the current emitted by a macrospin comprised of  $N = 20$  dipoles with precession frequency  $\Delta = 100\gamma_0$ , placed a height  $d = 10^{-3}v_F/\gamma_0$  away from a conductor with Fermi energy  $E_F = 10^6 \hbar \gamma_0/2$ . A video showing the evolution be found at [33].

the fast precession of the magnetic dipoles, the current distribution has the form of a spiral with radial periodicity  $v_f \Delta^{-1}$ . Finally, the wave packet of the emitted transverse-current wave has a width  $\propto v_F \gamma_0^{-1}/N$  since the drive is active only during the decay time  $\gamma_0^{-1}/N$ .

*Discussion.*— Finally, we discuss a few novelties relevant to the superradiance of NVs coupled to magnetic fluctuations of a material. First is that the height dependence offers an additional knob for inducing collective effects: if the NVs have separation smaller than their height, then they will show collective effects simply due to the magnetostatic coupling. Thus, even a paramagnet, with very short-range magnetic fluctuations, could induce collective relaxation simply due to the nonlocality of the magnetostatic coupling.

Furthermore, materials introduce both disorder and interaction effects, which might modify length scales at which correlated emission can occur. For example, the mean free path  $l$  in many common materials is shorter than  $v_F/\Delta$ , and the condition for superradiance will be modified: likely requiring  $a < l$ . In addition, a preliminary analysis of Fermi-liquid effects suggest realistic interactions will not qualitatively modify the above predictions. The exception is if there are strong enough interactions that a transverse-current zero-sound mode appears in the spectrum [36, 37]. Such zero-sound mode may provide an alternative bosonic excitation for collective emission.

Finally, the collective emission rate needs to be larger than any intrinsic relaxation process of the NVs. For room temperature conductors, the induced rate  $\gamma_0$  is measured [16, 17] to be larger than the intrinsic rate, with a magnitude around 1KHz for an NV placed 50nm away from the sample. Since classical noise scales lin-

early with temperature, these materials may effectively decouple at low temperature making it difficult to observe collective quantum effects due to a gas of conduction electrons. While this will pose problems for observing subradiance, superradiance describes the classical motion of the macrospin formed from the collection of magnetic-dipoles. Accordingly, temperature will only induce thermal noise in the collective relaxation process, and could be relatively small when the number of dipoles is large  $N \gg k_B T / \hbar \Delta$ .

*Acknowledgments*- We appreciate discussions with Shu Zhang and Jamir Marino. This work is supported by NSF under Grant No. DMR-2049979.

- 
- [1] R. H. Dicke, Coherence in spontaneous radiation processes, *Phys. Rev.* **93**, 99 (1954).
  - [2] N. Skribanowitz, I. P. Herman, J. C. MacGillivray, and M. S. Feld, Observation of dicke superradiance in optically pumped hf gas, *Phys. Rev. Lett.* **30**, 309 (1973).
  - [3] M. Gross, P. Goy, C. Fabre, S. Haroche, and J. M. Raimond, Maser oscillation and microwave superradiance in small systems of rydberg atoms, *Phys. Rev. Lett.* **43**, 343 (1979).
  - [4] M. A. Norcia, M. N. Winchester, J. R. K. Cline, and J. K. Thompson, Superradiance on the millihertz linewidth strontium clock transition, *Science Advances* **2**, e1601231 (2016).
  - [5] M. Scheibner, T. Schmidt, L. Worschech, A. Forchel, G. Bacher, T. Passow, and D. Hommel, Superradiance of quantum dots, *Nature Physics* **3**, 106 (2007).
  - [6] C. Liedl, F. Tebbenjohanns, C. Bach, S. Pucher, A. Rauschenbeutel, and P. Schneeweiss, Observation of superradiant bursts in a cascaded quantum system, *Phys. Rev. X* **14**, 011020 (2024).

- [7] P. Solano, P. Barberis-Blostein, F. K. Fatemi, L. A. Orozco, and S. L. Rolston, Super-radiance reveals infinite-range dipole interactions through a nanofiber, *Nature Communications* **8**, 1857 (2017).
- [8] C. Bradac, M. T. Johnsson, M. van Breugel, B. Q. Baragiola, R. Martin, M. L. Juan, G. K. Brennen, and T. Volz, Room-temperature spontaneous superradiance from single diamond nanocrystals, *Nature Communications* **8**, 1205 (2017).
- [9] A. Angerer, K. Streltsov, T. Astner, S. Putz, H. Sumiya, S. Onoda, J. Isoya, W. J. Munro, K. Nemoto, J. Schmiedmayer, and J. Majer, Superradiant emission from colour centres in diamond, *Nature Physics* **14**, 1168 (2018).
- [10] Q. Wu, Y. Zhang, X. Yang, S.-L. Su, C. Shan, and K. Mølmer, A superradiant maser with nitrogen-vacancy center spins, *Science China Physics, Mechanics & Astronomy* **65**, 217311 (2021).
- [11] B. Lemberger and D. D. Yavuz, Effect of correlated decay on fault-tolerant quantum computation, *Phys. Rev. A* **96**, 062337 (2017).
- [12] J. Zou, S. Zhang, and Y. Tserkovnyak, Bell-state generation for spin qubits via dissipative coupling, *Physical Review B* **106**, L180406 (2022).
- [13] A. Asenjo-Garcia, M. Moreno-Cardoner, A. Albrecht, H. J. Kimble, and D. E. Chang, Exponential improvement in photon storage fidelities using subradiance and “selective radiance” in atomic arrays, *Phys. Rev. X* **7**, 031024 (2017).
- [14] D. E. Chang, J. S. Douglas, A. González-Tudela, C.-L. Hung, and H. J. Kimble, Colloquium: Quantum matter built from nanoscopic lattices of atoms and photons, *Rev. Mod. Phys.* **90**, 031002 (2018).
- [15] X. Li, J. Marino, D. E. Chang, and B. Flebus, *A solid-state platform for cooperative quantum dynamics driven by correlated emission* (2024), [arXiv:2309.08991](https://arxiv.org/abs/2309.08991) [quant-ph].
- [16] S. Kolkowitz, A. Safira, A. A. High, R. C. Devlin, S. Choi, Q. P. Unterreithmeier, D. Patterson, A. S. Zibrov, V. E. Manucharyan, H. Park, and M. D. Lukin, Probing Johnson noise and ballistic transport in normal metals with a single-spin qubit, *Science* **347**, 1129 (2015).
- [17] A. Ariyaratne, D. Bluvstein, B. A. Myers, and A. C. B. Jayich, Nanoscale electrical conductivity imaging using a nitrogen-vacancy center in diamond, *Nature Communications* **9**, 2406 (2018).
- [18] J. M. Taylor, P. Cappellaro, L. Childress, L. Jiang, D. Budker, P. R. Hemmer, A. Yacoby, R. Walsworth, and M. D. Lukin, High-sensitivity diamond magnetometer with nanoscale resolution, *Nature Physics* **4**, 810 (2008).
- [19] E. Lee-Wong, R. Xue, F. Ye, A. Kreisel, T. van der Sar, A. Yacoby, and C. R. Du, Nanoscale Detection of Magnon Excitations with Variable Wavevectors Through a Quantum Spin Sensor, *Nano Lett.* **20**, 3284 (2020).
- [20] J.-P. Tetienne, N. Donschuk, D. A. Broadway, A. Stacey, D. A. Simpson, and L. C. L. Hollenberg, Quantum imaging of current flow in graphene, *Science Advances* **3**, e1602429 (2017).
- [21] S. Li, M. Huang, H. Lu, N. J. McLaughlin, Y. Xiao, J. Zhou, E. E. Fullerton, H. Chen, H. Wang, and C. R. Du, Nanoscale Magnetic Domains in Polycrystalline Mn<sub>3</sub>Sn Films Imaged by a Scanning Single-Spin Magnetometer, *Nano Lett.* **23**, 5326 (2023).
- [22] M. A. Ruderman and C. Kittel, Indirect exchange coupling of nuclear magnetic moments by conduction electrons, *Phys. Rev.* **96**, 99 (1954).
- [23] T. Kasuya, A theory of metallic ferro- and antiferromagnetism on zener’s model, *Progress of Theoretical Physics* **16**, 45 (1956).
- [24] K. Yosida, Magnetic properties of cu-mn alloys, *Phys. Rev.* **106**, 893 (1957).
- [25] K. Binder and A. P. Young, Spin glasses: Experimental facts, theoretical concepts, and open questions, *Rev. Mod. Phys.* **58**, 801 (1986).
- [26] F. Jelezko, T. Gaebel, I. Popa, M. Domhan, A. Gruber, and J. Wrachtrup, Observation of coherent oscillation of a single nuclear spin and realization of a two-qubit conditional quantum gate, *Phys. Rev. Lett.* **93**, 130501 (2004).
- [27] For an anisotropic Fermi surface, the largest wavenumber  $q$  depends on the orientation of  $\mathbf{q}$ . Correlated decay sensitive to  $k_F$  might then be able to probe the shape of the Fermi surface.
- [28] M. W. Doherty, N. B. Manson, P. Delaney, F. Jelezko, J. Wrachtrup, and L. C. Hollenberg, The nitrogen-vacancy colour centre in diamond, *Physics Reports* **528**, 1 (2013).
- [29] The NV qubit comprises two levels of an electronic triplet, and the coupling to the magnetic field is generally anisotropic.
- [30] S. Zhang and Y. Tserkovnyak, Flavors of magnetic noise in quantum materials, *Phys. Rev. B* **106**, L081122 (2022).
- [31] S. Chatterjee, P. E. Dolgirev, I. Esterlis, A. A. Zibrov, M. D. Lukin, N. Y. Yao, and E. Demler, Single-spin qubit magnetic spectroscopy of two-dimensional superconductivity, *Physical Review Research* **4**, L012001 (2022).
- [32] S. P. Kelly and Y. Tserkovnyak, *Superconductivity-enhanced magnetic field noise* (2024), [arXiv:2412.05465](https://arxiv.org/abs/2412.05465) [cond-mat.supr-con].
- [33] Supplemental material (2024), see Supplemental Material for additional details and data.
- [34] S. J. Masson, I. Ferrier-Barbut, L. A. Orozco, A. Browaeys, and A. Asenjo-Garcia, Many-body signatures of collective decay in atomic chains, *Phys. Rev. Lett.* **125**, 263601 (2020).
- [35] S. J. Masson and A. Asenjo-Garcia, Universality of dicke superradiance in arrays of quantum emitters, *Nature Communications* **13**, 2285 (2022).
- [36] V. Silin, Oscillations of a degenerate electron fluid, *Zh. Éksp. Teor. Fiz.* **35** (1958).
- [37] L. Gor’kov and I. Dzyaloshinskii, Feasibility of zero-sound oscillations in metals, *Sov. Phys. JETP* **17** (1963).

# Supplemental material for: Correlated emission of electron-current waves

Shane P. Kelly, Eric Kleinherbers, Yanyan Zhu, and Yaroslav Tserkovnyak

*Department of Physics and Astronomy and Mani L. Bhaumik Institute for Theoretical Physics,  
University of California, Los Angeles, CA 90095*

This Supplemental material first introduces a general model for magnetic dipoles interacting with bosonic and fermionic environments, discusses the projection of NV center spin-1 triplets to effective two-level systems, and analyzes the coupling to current fluctuations in two-dimensional conductors. Next, the document derives expressions for magnetic field fluctuations, relaxation rates, and discusses details regarding collective emission phenomena such as superradiance and subradiance. Finally it presents the response of electron currents to a decaying macrospin, including analytic and numerical results, and connects the dynamic and static current responses to established physical concepts like Landau diamagnetism. In addition to this document the supplemental material includes a video of the current emitted by the superradiant decay of a macrospin.

## CONTENTS

I. Model	1
A. Projection of the NV triplet to two levels	2
B. Bosonic and Fermionic Environments	2
1. Translation Symmetry	2
2. Rotation Symmetry	3
C. Oersted coupling to 2D current Fluctuations	3
II. Environment Fluctuations	4
A. Magnetic field noise from current fluctuations	4
1. Role of NV Orientation	5
2. Position dependence of non-local decay rates	5
III. Superradiance	5
1. Initial state: $ \psi\rangle =  +\rangle^{\otimes N}$	5
2. Initial state: $(\psi_+  +\rangle + \psi_-  -\rangle)^{\otimes N}$	6
A. Comparison to second-order photon-correlation function	6
B. Homogeneous distribution	6
1. Acceleration of decay process $\partial_t R$	7
2. Decay rate	7
IV. Subradiance	8
A. Homogeneous distribution of spins	8
V. Magnetic moment	9
VI. Current response	9
A. Current-current response	10
B. Dynamic response	11
C. Static response	12
References	12

## I. MODEL

In the Supplemental Material, we will consider a slightly more generic setting in which the ground state of the  $n$ th magnetic dipole points in a generic direction  $\hat{\mathbf{z}}_n$ , and defines a coordinate system  $\hat{\mathbf{x}}_n, \hat{\mathbf{y}}_n, \hat{\mathbf{z}}_n$ . The magnetic dipoles are described by Pauli spin operators,  $\boldsymbol{\sigma}_n = (\sigma_n^x, \sigma_n^y, \sigma_n^z)$ , whose dynamics are described by a Hamiltonian

$$H = \frac{\hbar\Delta}{2} \sum_n \sigma_n^z + \gamma_e \frac{\hbar}{2} \sum_n \mathbf{B}(\mathbf{r}_n) \cdot \boldsymbol{\sigma}_n + H_E \quad (1)$$

where  $\hbar\Delta$  is the energy spacing of the two levels,  $-\gamma_e$  is the gyromagnetic ratio of the magnetic dipole,  $\mathbf{B}(\mathbf{r}_n)$  is the magnetic field operator at the position of the  $n$ th dipole, and  $H_E$  is the Hamiltonian of the environment determining the dynamics of the magnetic fields in the absence of the dipoles.

### A. Projection of the NV triplet to two levels

In this section, we note that the magnetic levels of the NV are comprised of a spin-1 triplet and experiments are typical performed on two of the three levels. While the projection to two levels does not yield a spin-half dipole, the result can still be written in terms of Pauli operators. The spin-1 operator  $\mathbf{S}_n$  of the  $n$ th NV center can be written in the eigenbasis  $\{|0\rangle, |\uparrow\rangle, |\downarrow\rangle\}_n$ . Projecting onto the two-level subset with  $|+\rangle = |\uparrow\rangle$  and  $|-\rangle = |0\rangle$ , we can identify the Pauli matrices  $\sigma_n$  through the projection  $\mathbf{S}_n \rightarrow \frac{\hbar}{2} (\sqrt{2}\sigma_n^x, \sqrt{2}\sigma_n^y, 1 + \sigma_n^z)$ . Hence, the coupling to the magnetic field does not generically yield the Hamiltonian  $\frac{\hbar\gamma_{NV}}{2}\boldsymbol{\sigma} \cdot \mathbf{B}$  from Eq. (??). Instead, we obtain

$$\gamma_{NV}\mathbf{S}_n \cdot \mathbf{B}(\mathbf{r}_n) \rightarrow \frac{\hbar\gamma_{NV}}{2}\sigma_n^z B^z(\mathbf{r}_n) + \frac{\hbar\gamma_{NV}}{\sqrt{2}}(\sigma_n^x B^x(\mathbf{r}_n) + \sigma_n^y B^y(\mathbf{r}_n)), \quad (2)$$

which has an anisotropy between  $z$  and  $x, y$ . Accordingly, in Eq. (23), the replacement  $\gamma_e \rightarrow \gamma_{NV}$  should be made to determine the dephasing rates, while the replacement  $\gamma_e \rightarrow \sqrt{2}\gamma_{NV}$  should be made to determine the decay and excitation rates. Furthermore, if we prepare the system in the polarized state  $(|+\rangle + |-\rangle)/\sqrt{2}$ , the NV spin is not polarized along  $x$ , but partially points in the  $z$  direction  $\langle \mathbf{S} \rangle = (1/\sqrt{2}, 0, 1/2)$ . Similarly, we obtain  $\langle \mathbf{S} \rangle = 0$  in the ground state  $|-\rangle$ .

### B. Bosonic and Fermionic Environments

We consider two generic environments of volume  $V$ , one bosonic and the other fermionic, both with dispersion  $\hbar\omega_k$ . Both environments are quadratic with the Hamiltonians

$$H_b = \sum_{\mathbf{k}} \hbar\omega_k b_{\mathbf{k}}^\dagger b_{\mathbf{k}}, \quad H_f = \sum_{\mathbf{k}} \hbar\omega_k f_{\mathbf{k}}^\dagger f_{\mathbf{k}} \quad (3)$$

where  $b_{\mathbf{k}}$  and  $f_{\mathbf{k}}$  are the boson and fermionic creation operators corresponding to plane waves with wave vectors  $\mathbf{k}$ . Spin indices could be included, but are not important for the discussion below.

Bosons and fermions couple differently to the magnetic dipole: For bosons, we consider a linear coupling in which the magnetic field is proportional to the boson creation and annihilation operators

$$\mathbf{B}(\mathbf{r}) = \sum_{\mathbf{k}} \frac{\mathbf{g}_{\mathbf{k}}(\mathbf{r})}{\sqrt{V}} b_{\mathbf{k}} + h.c. \quad (4)$$

Such coupling is generic in quantum optics when the dipoles couple to boson modes. It is also relevant for NV centers coupled to magnons [1, 2]. In contrast, the fermionic environment must couple quadratically as the magnetic field is a bosonic operator:

$$\mathbf{B}(\mathbf{r}) = \sum_{\mathbf{k}, \mathbf{k}'} \frac{\mathbf{V}_{\mathbf{k}, \mathbf{k}'}(\mathbf{r})}{V} f_{\mathbf{k}}^\dagger f_{\mathbf{k}'}, \quad (5)$$

where  $V$  is the  $d$  dimensional volume in which the plane waves are quantized.

#### 1. Translation Symmetry

For a homogeneous coupling, the matrix elements satisfy

$$\begin{aligned} \mathbf{g}_{\mathbf{k}}(\mathbf{r} + \boldsymbol{\delta}) &= \mathbf{g}_{\mathbf{k}}(\mathbf{r}) e^{i\mathbf{k} \cdot \boldsymbol{\delta}} \\ \mathbf{V}_{\mathbf{k}, \mathbf{k}'}(\mathbf{r} + \boldsymbol{\delta}) &= \mathbf{V}_{\mathbf{k}, \mathbf{k}'}(\mathbf{r}) e^{i(\mathbf{k}' - \mathbf{k}) \cdot \boldsymbol{\delta}}, \end{aligned} \quad (6)$$



such that  $\mathbf{g}_{\mathbf{k}}(\mathbf{r}) = \mathbf{g}_{\mathbf{k}}(0)e^{i\mathbf{k}\cdot\mathbf{r}}$  and similarly for the fermion matrix elements. Thus, the magnetic fields at wave vector  $\mathbf{q}$ ,  $\mathbf{B}(\mathbf{q}) = \int_V d\mathbf{r} e^{-i\mathbf{q}\cdot\mathbf{r}} \mathbf{B}(\mathbf{r})$  are

$$\begin{aligned} \mathbf{B}(\mathbf{q}) &= \sqrt{V} \left( \mathbf{g}_{\mathbf{q}} b_{\mathbf{q}} + \mathbf{g}_{-\mathbf{q}}^* b_{-\mathbf{q}}^\dagger \right) \\ \mathbf{B}(\mathbf{q}) &= \sum_{\mathbf{k}} \mathbf{V}_{\mathbf{k}, \mathbf{k}+\mathbf{q}} f_{\mathbf{k}}^\dagger f_{\mathbf{k}+\mathbf{q}}, \end{aligned} \quad (7)$$

where we have defined  $\mathbf{g}_{\mathbf{q}} = \mathbf{g}_{\mathbf{q}}(\mathbf{r} = 0)$  and  $\mathbf{V}_{\mathbf{k}, \mathbf{k}+\mathbf{q}} = \mathbf{V}_{\mathbf{k}, \mathbf{k}+\mathbf{q}}(\mathbf{r} = 0)$  for bosons and fermions respectively. The corresponding real-space magnetic-field operators are given in the main text.

## 2. Rotation Symmetry

We now assume the environment is also symmetric around an axis  $\hat{\mathbf{d}}$ , which is generically not the orientation of the dipoles  $\hat{\mathbf{z}}_n$ . In the case of NVs placed above a conductor,  $\hat{\mathbf{d}}$  is the direction perpendicular to the plane of the material. If  $\hat{\mathbf{x}}$ ,  $\hat{\mathbf{y}}$  and  $\hat{\mathbf{d}}$  form a right-handed basis, then the magnetic fields  $B^\pm(\mathbf{q}) = B^x(\mathbf{q}) \pm B^y(\mathbf{q})$  transform as  $B^\pm(\mathbf{q}) \rightarrow B^\pm(\mathbf{q}_\phi) e^{\pm i\phi}$  under a rotation by  $\phi$  around the  $\hat{\mathbf{d}}$  axis (where  $\mathbf{q}_\phi$  is the vector  $\mathbf{q}$  rotated around  $\hat{\mathbf{d}}$  by  $\phi$ ). Thus, the boson couplings will satisfy

$$\begin{aligned} g_{\mathbf{q}_\phi}^\pm &= g_{\mathbf{q}}^\pm e^{\pm i\phi} \\ g_{\mathbf{q}_\phi}^d &= g_{\mathbf{q}}^d, \end{aligned} \quad (8)$$

and the fermion couplings will satisfy

$$\begin{aligned} V_{\mathbf{k}_\phi, \mathbf{k}_\phi + \mathbf{q}_\phi}^\pm &= V_{\mathbf{k}, \mathbf{k} + \mathbf{q}}^\pm e^{\pm i\phi} \\ V_{\mathbf{k}_\phi, \mathbf{k}_\phi + \mathbf{q}_\phi}^d &= V_{\mathbf{k}, \mathbf{k} + \mathbf{q}}^d. \end{aligned} \quad (9)$$

## C. Oersted coupling to 2D current Fluctuations

For a concrete example, we consider the situation when the magnetic-dipoles are located in a two-dimensional plane at a height  $d$  above a two-dimensional conductor. Consistent with previous estimates [3], we neglect couplings to magnetization noise produced by electron-spin fluctuations and only consider magnetic fields produced by current fluctuations. The two-dimensional current density has the form

$$\mathbf{J}(\mathbf{q}) = \int_V d\rho e^{-i\mathbf{q}\cdot\boldsymbol{\rho}} \mathbf{J}(\boldsymbol{\rho}) = -\frac{e\hbar}{m} \sum_{\sigma, \mathbf{k}} \left( \mathbf{k} - \frac{\mathbf{q}}{2} \right) f_{\sigma, \mathbf{k}-\mathbf{q}}^\dagger f_{\sigma, \mathbf{k}}, \quad (10)$$

where  $e$  is the magnitude of the electron charge. The corresponding magnetic field at wave vector  $\mathbf{q}$  is given by [3]

$$\mathbf{B}(\mathbf{r}) = \int_{\mathcal{R}_2} \frac{d^2\mathbf{q}}{(2\pi)^2} e^{i\mathbf{q}\cdot\mathbf{r}} \mathbf{G}(\mathbf{q}) \times \mathbf{J}(\mathbf{q}) \quad (11)$$

where

$$\mathbf{G}(\mathbf{q}) = \frac{2\pi}{c} e^{-qd} \left( i\hat{\mathbf{q}} - \text{sign}(d)\hat{\mathbf{d}} \right), \quad (12)$$

where  $\hat{\mathbf{d}}$  is the direction perpendicular to the plane, and  $\text{sign}(d)$  is determined by the side of the plane being considered.

Defining a right-handed basis by  $\hat{\mathbf{q}}_\perp, \hat{\mathbf{q}}, \hat{\mathbf{d}}$ , we decompose the current into a longitudinal component  $\hat{\mathbf{q}} \cdot \mathbf{J}(\mathbf{q})$  and a transverse component  $\hat{\mathbf{q}}_\perp \cdot \mathbf{J}(\mathbf{q})$ . The Fermi gas only supports longitudinal current in a small region of phase space near  $q \approx \omega/v_F$  and  $q \approx 2k_F$ . Furthermore, the Coulomb interaction suppresses longitudinal fluctuations for frequencies below the plasma frequency. Accordingly, we only consider contributions from transverse fluctuations. The magnetic field from this component is

$$\mathbf{B}(\mathbf{q}) = \frac{2\pi e\hbar}{cm} e^{-qd} (\hat{\mathbf{q}} + i\hat{\mathbf{d}}) \sum_{\sigma, \mathbf{k}} \hat{\mathbf{q}}_\perp \cdot \mathbf{k} f_{\sigma, \mathbf{k}}^\dagger f_{\sigma, \mathbf{k}+\mathbf{q}}, \quad (13)$$

where we have assumed  $d > 0$  and evaluated the cross product in Eq. (11) using only the transverse component  $(\hat{\mathbf{d}} - i\hat{\mathbf{q}}) \times \hat{\mathbf{q}}_\perp = (\hat{\mathbf{q}} + i\hat{\mathbf{d}})$ . Thus, the coupling matrix is given by

$$\mathbf{V}_{\mathbf{k}, \mathbf{k}+\mathbf{q}}(0) = (\hat{\mathbf{q}} + i\hat{\mathbf{d}}) \frac{2\pi e\hbar}{cm} e^{-qd} (\hat{\mathbf{q}}_\perp \cdot \mathbf{k}), \quad (14)$$

and satisfies the rotational symmetry relations in Eq. (9).

## II. ENVIRONMENT FLUCTUATIONS

The magnetic field fluctuations  $C^{\alpha\beta}(\mathbf{q}, \omega)$ , are qualitatively different for fermions vs bosons. At a fixed frequency, and in thermal equilibrium, bosonic fluctuations are significantly more constrained:

$$C^{\alpha\beta}(\omega, \mathbf{q}) = 2\pi \left[ g_{\mathbf{q}}^\alpha g_{\mathbf{q}}^{*\beta} (1 + n_{\mathbf{q}}) \delta(\omega - \omega_{\mathbf{q}}) + g_{-\mathbf{q}}^\beta g_{-\mathbf{q}}^{*\alpha} n_{-\mathbf{q}} \delta(\omega + \omega_{-\mathbf{q}}) \right], \quad (15)$$

where  $n_{\mathbf{q}}$  is the Bose-Einstein distribution. In contrast, fermion fluctuations occur for a continuum of wave vectors for a fixed frequency,

$$C^{\alpha\beta}(\omega, \mathbf{q}) = \int \frac{d^d \mathbf{k}}{(2\pi)^{d-1}} V_{\mathbf{k}, \mathbf{k}+\mathbf{q}}^\alpha V_{\mathbf{k}+\mathbf{q}, \mathbf{k}}^\beta n_{\mathbf{k}} (1 - n_{\mathbf{k}+\mathbf{q}}) \delta(\omega + \omega_{\mathbf{k}} - \omega_{\mathbf{k}+\mathbf{q}}) + F^\alpha F^\beta (2\pi)^{d+1} \delta(\omega) \delta(\mathbf{q}), \quad (16)$$

where  $n_{\mathbf{k}}$  is now the Fermi-Dirac distribution and  $F^\gamma = \int d^d \mathbf{k} V_{\mathbf{k}, \mathbf{k}}^\gamma n_{\mathbf{k}} / (2\pi)^d$ . The last term is the static homogeneous response and does not contribute to the dynamics of the dipoles.

For simplicity, we first assume momentum and direction independent couplings  $V_{\mathbf{k}, \mathbf{k}+\mathbf{q}}^\alpha = \mathcal{V}$ . In this case, the integral for the fermion fluctuations in Eq. (16) can be evaluated at zero temperature as

$$C^{\alpha\beta}(\omega, \mathbf{q}) = \begin{cases} \frac{\sqrt{2}\mathcal{V}^2 m^{3/2}}{\pi \hbar^2 q} \left( \sqrt{E_F - E(q, \omega)} - \sqrt{E_F - \hbar\omega - E(q, \omega)} \right) & , E(q, \omega) < E_F - \hbar\omega \\ \frac{\sqrt{2}\mathcal{V}^2 m^{3/2}}{\pi \hbar^2 q} \sqrt{E_F - E(q, \omega)} & , E_F - \hbar\omega < E(q, \omega) < E_F \\ 0 & , E_F < E(q, \omega) \end{cases} \quad (17)$$

where

$$E(q, \omega) = \frac{\hbar^2}{8m} \frac{(q_\omega^2 - q^2)^2}{q^2} \text{ and } q_\omega = \sqrt{\frac{2m\omega}{\hbar}}, \quad (18)$$

and we have assumed a dispersion  $\omega_{\mathbf{k}} = \hbar k^2 / 2m$ . At small frequency  $\hbar\omega \ll E_F$ , the fluctuations are finite in an interval determined by  $E(q, \omega) < E_F$  or  $\omega/v_F < q < 2k_F$ . At zero temperature,  $C^{\alpha\beta}(\omega, \mathbf{q}) = 0$  for  $\omega < 0$ .

### A. Magnetic field noise from current fluctuations

The magnetic-field fluctuations produced by the current can also be evaluated exactly for an isotropic 2D Fermi surface:

$$C^{\alpha\beta}(\omega, \mathbf{q}) = (\hat{\mathbf{q}}_\alpha + i\hat{\mathbf{d}}_\alpha) (\hat{\mathbf{q}}_\beta - i\hat{\mathbf{d}}_\beta) e^{-2dq} \left( \frac{2ev_f}{c} \right)^2 \frac{\pi m}{\hbar} \frac{k_F}{q} C(q, \omega)$$

where

$$C(q, \omega) = \frac{2}{3E_F^{3/2}} \left[ (E_F - E(q, \omega))^{3/2} - (E_F - \hbar\omega - E(q, \omega))^{3/2} \right] \quad (19)$$

if  $E(q, \omega) < E_F - \hbar\omega$ , and has a similar generalization for  $E(q, \omega) > E_F$  and  $E_F - \hbar\omega < E(q, \omega) < E_F$  as in Eq. (17). The main difference is the 3/2 v.s. 1/2 exponent. Note, we have included a factor of 2 for the spin degrees of freedom.

In the range  $\omega/v_F \ll q \ll k_F$ , we can approximate  $E(\omega, \mathbf{q}) \approx \hbar^2 q^2 / 8m$  and make an expansion in both  $E(q, \omega) \ll E_F$  and  $E(q, \omega) + \hbar\omega \ll E_F$ . This yields

$$C(q, \omega) \approx \frac{\hbar\omega}{E_F}. \quad (20)$$

### 1. Role of NV Orientation

We now determine how the NV orientations affect the relaxation rates. As above, we consider the dipoles to point in the direction  $\hat{\mathbf{z}}_n$ , with  $\hat{\mathbf{x}}_n, \hat{\mathbf{y}}_n, \hat{\mathbf{z}}_n$  forming a right-handed basis. The relaxation rates  $\gamma_{nm} = \gamma_e^2/4 \int d\mathbf{q}/(2\pi)^2 C^{-+}(\omega, \mathbf{q})$  are then determined by

$$C^{-+}(\omega, \mathbf{q}) = F_{nm} e^{-2d\mathbf{q}} \left( \frac{2ev_f}{c} \right)^2 \frac{\pi m}{\hbar} \frac{k_F}{q} C(q, \omega) \quad (21)$$

where

$$F_{nm} = (\hat{\mathbf{x}}_n - i\hat{\mathbf{y}}_n) \cdot (\hat{\mathbf{q}} + i\hat{\mathbf{d}}) (\hat{\mathbf{x}}_m + i\hat{\mathbf{y}}_m) \cdot (\hat{\mathbf{q}} - i\hat{\mathbf{d}}) \quad (22)$$

contains the orientation dependence. In the simplest configuration, NVs point perpendicular to the plane  $\hat{\mathbf{z}}_n = \hat{\mathbf{d}}$ , and we find  $F_{nm} = 1$ . A numerical evaluation of the magnetic noise is shown in Fig. 2(a) of the main text.

A more interesting example is when the dipoles point parallel to the plane. Taking  $\hat{\mathbf{x}}, \hat{\mathbf{y}}$  and  $\hat{\mathbf{d}}$  to form a right-handed basis, then the parallel configuration is described by  $\hat{\mathbf{z}}_n = \hat{\mathbf{x}}$ ,  $\hat{\mathbf{x}}_n = \hat{\mathbf{y}}$  and  $\hat{\mathbf{y}}_n = \hat{\mathbf{d}}$  for all  $n$ . In this case, the coupling is not inversion symmetric  $F_{nm} = (1 + \hat{\mathbf{y}} \cdot \hat{\mathbf{q}})^2$ , and waves moving in the  $\hat{\mathbf{y}}$  direction couple more strongly than those moving in the  $-\hat{\mathbf{y}}$  direction. Finally, if the orientation of the NVs depends on position, the matrix  $F_{nm}$  will generally be complex but Hermitian.

### 2. Position dependence of non-local decay rates

In the case  $\hat{\mathbf{z}}_n = \hat{\mathbf{d}}$ , the integral over the azimuth can be performed and yields

$$\gamma(r) = \left( \frac{\gamma_e}{2} \right)^2 \int \frac{q dq}{2\pi} J_0(qr) C^{-+}(\omega, q), \quad (23)$$

where  $J_0(x)$  is the zeroth Bessel function of the first kind, and  $r = |\mathbf{r}_n - \mathbf{r}_m|$  is the distance between the two dipoles. The numerical integration of this equation is shown in Fig. 2(b) of the main text.

## III. SUPERRADIANCE

Correlated emission occurs when the nonlocal rates  $\gamma_{nm}$  are finite. Depending on the initial state, the relaxation process can be slower (subradiance) or faster (superradiance) than for independent emission. We will now determine the conditions for superradiance. While coherent effects and dephasing can and do interrupt superradiance, we will neglect these terms to identify the necessary conditions superradiance places on the relaxation rates  $\gamma_{nm}$  and on the corresponding bosonic or fermionic fluctuations. In addition, we will assume that all NVs point perpendicular to the plane  $\hat{\mathbf{z}}_n = \hat{\mathbf{d}}$ . The adjoint master equation for correlated loss is

$$\partial_t O = \frac{1}{2} \sum_{nm} \gamma_{nm} (\sigma_m^+ [O, \sigma_n^-] + [\sigma_m^+, O] \sigma_n^-). \quad (24)$$

In the limit of uncorrelated emission  $\gamma_{nm} \ll \gamma_{nn} = \gamma_0$  for  $m \neq n$ , the dipoles decay independently. The  $\hat{\mathbf{z}}$  component of each dipole decays as  $\langle \sigma_n^z(t) \rangle / 2 = P_1(0) e^{-\gamma_0 t} - 1/2$ , where  $P_1(0)$  is the excited-state population at  $t = 0$ . Thus, the decay rate of the total spin in the  $\hat{\mathbf{z}}$  direction  $S^z = \hbar \sum_k \sigma_k^z / 2$  obeys

$$R = -\partial_t \langle S^z \rangle / \hbar = N P_1(0) \gamma_0 e^{-\gamma_0 t}. \quad (25)$$

Furthermore, this rate decreases in time as the dipoles decay  $\partial_t R = -N P_1(0) \gamma_0^2 < 0$ . Below we will use deviation from these behaviors as an indication of cooperative effects.

### 1. Initial state: $|\psi\rangle = |+\rangle^{\otimes N}$

For an initial state fully polarized  $P_1(0) = 1$  in the excited state, the decay rates for independent and collective emission are the same  $R(t=0) = N\gamma_0$ . For this initial state, collective emission is distinguished at early times by

a decay process that accelerates as many-body coherences develop. Neglecting coherent, excitation and dephasing processes, the rate of change of the decay rate is given by

$$\begin{aligned}\partial_t R(t=0) &= - \sum_{nmk} \frac{\gamma_{nm}}{\hbar} \text{tr} \left[ S^z \sigma_n^- \partial_t \rho \sigma_m^+ - S^z \frac{1}{2} \{ \sigma_m^+ \sigma_n^-, \partial_t \rho \} \right] \\ &= \sum_{n \neq m} \gamma_{nm} \gamma_{mn} - \sum_n (\gamma_{nn})^2,\end{aligned}\tag{26}$$

where the second equality holds for an initial state that is fully polarized in  $\hat{z}$  direction. For independent emission, the decay-rate matrix  $\gamma_{nm} = \gamma_0 \delta_{nm}$  yields  $\partial_t R = -N\gamma_0^2$ , and implies the decay process slows as time evolves. In contrast, correlated emission will occur for a constant decay-rate matrix  $\gamma_{nm} = \gamma_0$  for all  $n$  and  $m$ . For this case, the decay process accelerates in time as  $\partial_t R = N(N-2)\gamma_0^2$ . This was the limit originally discussed by Dicke [4], and leads to a maximum decay rate  $\max_t R(t) \propto N^2$  known as the superradiance burst.

$$2. \text{ Initial state: } (\psi_+ |+\rangle + \psi_- |-\rangle)^{\otimes N}$$

For generic decay-rate matrix  $\gamma_{nm}$ , the maximum decay occurs after an initial decay in which spins develop collective coherence. To estimate a lower bound on the maximum decay rate [5], we consider the initial decay of a state with  $N$  dipoles prepared in product state

$$|\psi\rangle = (\psi_+ |+\rangle + \psi_- |-\rangle)^{\otimes N},\tag{27}$$

where  $\sigma^z |\pm\rangle = \pm |\pm\rangle$ . The decay rate is given as

$$R = \sum_k \gamma_{kk} |\psi_+|^2 + \sum_{n \neq m} \gamma_{nm} |\psi_+ \psi_-|^2,\tag{28}$$

for dipoles prepared in the  $+1$  eigenstate of  $\sigma^x$ , we find

$$R = \frac{1}{2} \sum_k \gamma_{kk} + \frac{1}{2} \sum_{n \neq m} \gamma_{nm}.\tag{29}$$

### A. Comparison to second-order photon-correlation function

In Ref. [6], the authors use the second-order photon-correlation function  $g^2(t=0)$  at the initial time as a condition for superradiance. They provide the second-order photon-correlation function as

$$g^2(t=0) = \frac{\sum_{\nu, \mu} \gamma_\nu \gamma_\mu \langle O_\nu^\dagger O_\mu^\dagger O_\mu O_\nu \rangle}{\left( \sum_\nu \gamma_\nu \langle O_\nu^\dagger O_\nu \rangle \right)^2},\tag{30}$$

where  $\gamma_\nu$  are the eigenvalues of the decay-rate matrix  $\gamma_{nm}$ , and  $O_\nu = \sum_m \alpha_{\nu, m} \sigma_m^-$  are the diagonal jump operators determined by the  $\nu$ th eigenvector  $\alpha_{\nu, m}$  of the decay-rate matrix. Their condition for superradiance, that the emission of the first-photon is positively correlated with that of the second  $g^2(t=0) > 1$ , is equivalent to ours  $\partial_t R(t=0) > 0$ . This is proven algebraically by substitution of  $O_\nu = \sum_m \alpha_{\nu, m} \sigma_m^-$  in to Eq. (30), and by using of the relation  $\gamma_{nm} = \sum_\nu \gamma_\nu \alpha_{\nu, n} \alpha_{\nu, m}^*$ , to obtain the expression in Eq. (26) appearing on the right-hand side of the inequality of  $\partial_t R(t=0) > 0$ . In addition, we used the relation  $\langle \sigma_r^+ \sigma_n^+ \sigma_m \sigma_s \rangle = (\delta_{nm} \delta_{rs} + \delta_{ns} \delta_{rm}) (1 - \delta_{ms})$

### B. Homogeneous distribution

We now consider dipoles distributed homogeneously in a two-dimensional region of size  $A$  and at a fixed height  $d$ .



### 1. Acceleration of decay process $\partial_t R$

The change in the decay rate  $\partial_t R$  depends on the two terms in Eq. (26). The term  $-\sum_n \gamma_{nn}^2 = -N\gamma_0^2$  does not depend on the distribution of dipoles for a homogeneous magnetic-field environment. The term,  $\sum_{n \neq m} |\gamma_{nm}|^2$  does, and when treating the magnetic field noise in momentum space, the dependence shows up in a factor similar to the form factor in scattering theory:

$$\sum_{n \neq m} \left\langle e^{i(\mathbf{q}_1 - \mathbf{q}_2) \cdot (\mathbf{r}_n - \mathbf{r}_m)} \right\rangle = \frac{N^2}{A} \int d^2 \mathbf{r} e^{i\mathbf{r} \cdot (\mathbf{q}_1 - \mathbf{q}_2)} g(r), \quad (31)$$

where  $g(r)$  is the pair-correlation function. At low density, the NVs are spaced far enough apart that  $g(r) \approx 1$ . In this limit, the integral over position can be taken and yields an initial change in the decay rate as

$$\partial_t R \approx N \left( \frac{\gamma_e}{2} \right)^4 \int \frac{d^2 \mathbf{q}_1 d^2 \mathbf{q}_2}{(2\pi)^4} C^{-+}(\omega, \mathbf{q}_1) C^{-+}(\omega, \mathbf{q}_2) \left( \frac{N}{A} (2\pi)^2 \delta(\mathbf{q}_1 - \mathbf{q}_2) - 1 \right). \quad (32)$$

Upon rearrangement, this can be simply expressed as

$$\frac{\partial_t R}{N\gamma_0^2} = n\pi\lambda_{\text{SR}}^2 - 1 \quad (33)$$

where  $n = N/A$  is the two-dimensional density of dipoles, we have assumed an isotropic noise  $C^{-+}(\omega, \mathbf{q}) = C^{-+}(\omega, q)$ , and define  $\lambda_{\text{SR}}$  as the length scale at which correlated emission occurs:

$$\pi\lambda_{\text{SR}}^2 = \frac{1}{C^{-+}(\Delta)^2} \int \frac{qdq}{2\pi} \tilde{C}(\Delta, q)^2, \quad (34)$$

where  $C^{-+}(\Delta) = \int dq q C^{-+}(\omega, q)/(2\pi)$  is the local spectral density at frequency  $\Delta$ .

For the homogeneous distribution, the acceleration  $\partial_t R/N\gamma_0^2$  is thus larger by an amount  $n\pi\lambda_{\text{SR}}^2$ , equal to the number of particles in the correlation region of size  $\pi\lambda_{\text{SR}}^2$ . This is in contrast to Dicke superradiance, where the acceleration is increased by the total number of particles  $N$ . For concreteness, consider the simple model for magnetic noise  $C^{-+}(\Delta, \mathbf{q}_1) = C\theta(q_{\text{max}} - |\mathbf{q}|)$  in which magnet noise is cutoff above the scale  $q_{\text{max}}$ . This yields the correlated emission length scale  $\lambda_{\text{SR}}^2 = 4q_{\text{max}}^{-2}$ , as might be expected.

### 2. Decay rate

Determining the decay rate for the dipoles initialized in a  $\sigma^x$  eigenstate is more subtle. For a homogeneous environment, we find

$$R \approx \frac{N}{2} \gamma_0 + \frac{N^2}{2A} \int d^2 \mathbf{r} g(r) \gamma(r), \quad (35)$$

where  $g(r)$  is again the pair-correlation function, and the approximation becomes better in the large  $N$  limit. For a homogeneous low-density distribution, we approximate  $g(r) \approx 1$  in an infinite volume and obtain

$$R = \frac{N}{2} \gamma_0 + \frac{N}{2} n \left( \frac{\gamma_e}{2} \right)^2 C^{-+}(\Delta, \mathbf{q} = 0). \quad (36)$$

The second term vanishes if the magnetic-field correlations lack a  $\mathbf{q} = 0$  component at finite frequency  $\Delta$ . In this case, there is no collective enhancement due to a cancellation from oscillatory contributions from dipoles with large separation. For realistic configurations, disorder in both NV location and the nearby material will prevent this exact cancellation. Therefore, we consider how the rate scales with the area  $A$  occupied by the dipoles:

$$R \approx \frac{N}{2} \gamma_0 + N\pi n \int_0^{\sqrt{A}} r dr \gamma(r). \quad (37)$$

As an example, we consider  $\gamma(r) = \gamma_0(r_0/r)^\alpha$  above a scale  $r_0$ , and constant below that scale. For  $\alpha < 2$ , the dominant term grows with  $A$  as

$$R \approx \frac{N\pi}{2-\alpha} n\gamma_0 A^{1-\alpha/2} r_0^\alpha, \quad (38)$$

and there will be a superradiant burst. Otherwise, for  $\alpha > 2$ , the total decay-rate is similar to the independent rate  $R \approx N\gamma_0/2$ . In two dimensions, transverse current fluctuations generate magnetic-field noise with  $\alpha = 1$  as discussed in the main text.

#### IV. SUBRADIANCE

Subradiance is most well understood in the single-excitation sector. Here, the density matrix is described by a single-excitation wave function  $|\psi(t)\rangle$  and the ground state:

$$\rho(t) = |\psi(t)\rangle \langle\psi(t)| + P_0(t) |0\rangle \langle 0| \quad (39)$$

where  $|0\rangle$  is the  $-1$  eigenstate for all  $\sigma_n^z$  operators, and the single-excitation wave function has the form

$$|\psi(t)\rangle = \sum_n \psi_n(t) \sigma_n^+ |0\rangle, \quad (40)$$

with decaying normalization  $P_1(t) = 1 - P_0(t) = \sum_n |\psi_n(t)|^2$ . Substitution of  $\rho(t)$  into the Lindblad equation yields

$$\partial_t \psi_m(t) = -\frac{1}{2} \sum_n \gamma_{nm} \psi_n(t). \quad (41)$$

The eigenvalue  $\gamma_k$  of the decay-rate matrix  $\gamma_{nm}$  is the decay rate of the  $k$ th single-excitation eigenstate: The amplitude of the excitation decays as  $e^{-\gamma_k t/2}$  such that  $P_0(t) = 1 - e^{-\gamma_k t}$ . The two dipole decay-rate matrix

$$\gamma_{nm} = \begin{pmatrix} \gamma_0 & \gamma_a \\ \gamma_a & \gamma_0 \end{pmatrix} \quad (42)$$

has eigenvalues  $\gamma_0 \pm \gamma_a$  corresponding to a dark  $(-)$  and a bright state  $(+)$ .

##### A. Homogeneous distribution of spins

We now consider the case in which a collection of  $N$  magnetic dipoles are randomly distributed within a finite square region with density  $n = a^{-2}$ . In this case, the single-excitation decay rates are randomly distributed due to disorder in the position of the magnetic dipole locations (a homogeneous distribution in the square region). When all magnetic dipoles have a spacing  $a < \lambda_F \sqrt{N}$ , the decay rate matrix is a constant  $\gamma_{nm} \approx \gamma_0$ , and the spectrum contains one single-excitation eigenvector with a collective loss rate of  $N\gamma_0$  and  $N - 1$  darkstates with loss rate  $\approx 0$ .

As the spacing increases, some dipoles are separated from each other with separation  $r > \lambda_F$ , but subradiance remains so long as the average spacing is small  $a < \lambda_F$ . Once the average spacing is larger than the Fermi wavelength, subradiance diminishes. In Fig. 1, we show subradiance is lost slowly. For  $\lambda_F < a < 10\lambda_F$  dark states with  $\gamma_k < 0.1$  remain in the system, but become more and more rare. Then for  $a > 10\lambda_F$ , the slowest decaying eigenstate has a small decay but still comparable to the independent rate  $\gamma_0$ . Furthermore, for  $a > \lambda_F$ , a preliminary investigation into the spacial distribution of the darkstates shows that the subradiant states are all approximately singlets between two dipoles with separation  $r < \lambda_F$ . Since the mean spacing  $a > \lambda_F$  is large, these states are rare but still occur at a finite density decreasing with increasing mean spacing  $a$ .

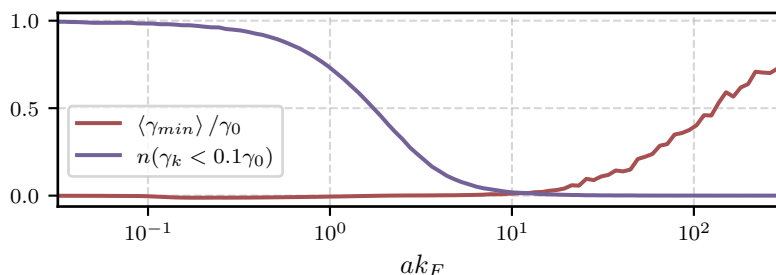


FIG. 1. Statistics of single-excitation decay rates  $\gamma_k$  (eigenvalues of the decay-rate matrix  $\gamma_{nm}$ ). The figure shows both  $\langle \gamma_{min} \rangle / \gamma_0$ , the smallest decay rate in the system averaged over disorder realizations, and  $n(\gamma_k < 0.1\gamma_0)$  the proportion of eigenvalues that are smaller than one 10th the independent rate  $\gamma_k < 0.1\gamma_0$ . The decay rates were evaluated for  $N = 500$  dipoles, and the plotted quantities were averaged over 50 disorder realizations.

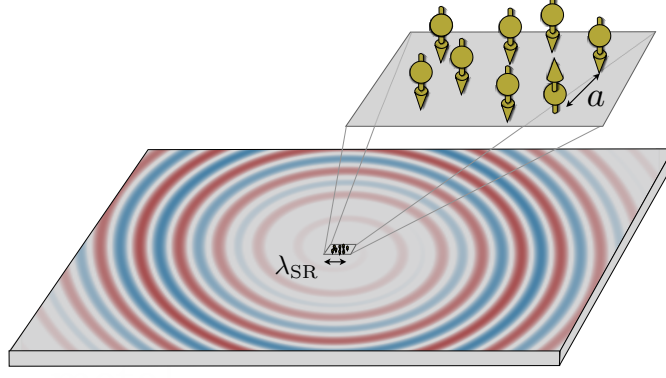


FIG. 2. Superradiance of electron current wave (blue and red) through the decay of the ensemble of dipoles (yellow). The current wave takes the form of a travelling spiral with two arms, where the currents are circulating clockwise (blue) and counterclockwise (red).

## V. MAGNETIC MOMENT

In this section, we review the physics of correlated emission in the Dicke limit, where the decay-rate matrix is constant,  $\gamma_{nm} = \gamma_0$ . The dynamics of the collective spin operator  $\mathbf{S} = \frac{\hbar}{2} \sum_n \boldsymbol{\sigma}_n$  is obtained from the adjoint Lindblad equation from Eq. (24). Defining  $S^\pm = S^x \pm iS^y$ , we obtain the coupled equations in the rotating frame:

$$\begin{aligned} \hbar \partial_t S^z &= -\gamma_0 S^+ S^-, \\ \hbar \partial_t S^+ &= \gamma_0 S^+ S^z, \\ \hbar \partial_t S^- &= \gamma_0 S^- S^z. \end{aligned} \quad (43)$$

This equation can be rewritten into the vector form:

$$\hbar \partial_t \mathbf{S} = -\gamma_0 \mathbf{S} \times (\hat{\mathbf{z}} \times \mathbf{S}) - \hbar \frac{\gamma_0}{2} (\hat{\mathbf{x}} - i\hat{\mathbf{y}}) S^+ - \hbar \gamma_0 \hat{\mathbf{z}} S^z, \quad (44)$$

where the first term can be identified as Landau-Lifshitz damping, which becomes dominant for large spins,  $N \gg 1$ . Transforming back to the lab frame and using the mean-field approximation, we obtain for the expectation value

$$\partial_t \langle \mathbf{S} \rangle \approx -\Delta \hat{\mathbf{z}} \times \langle \mathbf{S} \rangle - \gamma_0 \langle \mathbf{S} \rangle \times (\hat{\mathbf{z}} \times \langle \mathbf{S} \rangle). \quad (45)$$

Here, we used that for large spins,  $N \gg 1$ , Landau-Lifshitz damping  $\propto N^2$  dominates. The exact solution to this equation is given by

$$\begin{aligned} \langle S^x \rangle &= \frac{N\hbar}{2} \cos(\Delta t) \operatorname{sech}\left(\frac{N\gamma_0}{2} t\right), \\ \langle S^y \rangle &= -\frac{N\hbar}{2} \sin(\Delta t) \operatorname{sech}\left(\frac{N\gamma_0}{2} t\right), \\ \langle S^z \rangle &= -\frac{N\hbar}{2} \tanh\left(\frac{N\gamma_0}{2} t\right), \end{aligned} \quad (46)$$

where the initial condition is fully polarized in the  $\hat{\mathbf{x}}$  direction,  $\langle \mathbf{S} \rangle(t=0) = (\frac{N\hbar}{2}, 0, 0)$ .

## VI. CURRENT RESPONSE

In this section, we derive the electron current response  $\mathbf{J}(\mathbf{r}, t)$  to the magnetic field generated by the ensemble of magnetic dipoles. A movie illustrating the time evolution of the current as the spin ensemble decays is provided at

[7]. As above, we only consider the transverse current  $J_\perp(\mathbf{q}, \omega) = \hat{\mathbf{q}}_\perp \cdot \mathbf{J}(\mathbf{q}, \omega)$ , which we determine via the Kubo formula [8] for the transverse-current response  $J_\perp$  to the magnetic field  $\nabla \times \mathbf{A}$ :

$$\langle J_\perp(\mathbf{q}, \omega) \rangle = - \left[ \frac{1}{\hbar} G_0^R(\mathbf{q}, \omega) + \frac{e^2 \rho_e}{m} \right] \hat{\mathbf{q}}_\perp \cdot \mathbf{A}(\mathbf{q}, \omega)/c, \quad (47)$$

where the first term is the “paramagnetic” current  $\mathbf{J}^{\text{para}}$  given by the retarded Green’s function  $G_0^R$  of current-current fluctuations and the second term is the “diamagnetic” current  $\mathbf{J}^{\text{dia}}$ , and  $\rho_e = k_F^2/2\pi$  is the 2D electron density.

The vector potential  $\mathbf{A}$  in the plane of the 2D electron gas can be derived from the magnetic interaction  $H_{\text{int}} = -\mathbf{m} \cdot \mathbf{B} = -\frac{1}{c} \int d^2\mathbf{r} \mathbf{J} \cdot \mathbf{A}$ . Using Eq. (11), we obtain

$$\mathbf{A}(\mathbf{q}, \omega) = c\mathbf{G}(\mathbf{q}) \times \mathbf{m}(\omega), \quad (48)$$

where  $\mathbf{G}$  is the magnetostatic Green’s function defined in Eq. (12),  $\mathbf{m}(\omega) = -\gamma_e \langle \mathbf{S}(\omega) \rangle$  is the magnetic moment of the decaying macrospin, and we have applied the Coulomb gauge  $\nabla \cdot \mathbf{A} = 0$ . The evolution of the macrospin  $\langle \mathbf{S}(\omega) \rangle(t)$  is given by Eq. (46).

In total the response of the current to the decaying macrospin is written as

$$\langle J_\alpha(\mathbf{r}, t) \rangle = \int \frac{d\omega}{2\pi} e^{-i\omega t} \chi_{\alpha\beta}(\mathbf{r}, \omega) \langle S_\beta(\omega) \rangle \quad (49)$$

with the response function  $\chi_{\alpha\beta}$  found as:

$$\chi_{\alpha\beta}(\mathbf{r}, \omega) = \frac{2\pi\gamma_e}{c} \int \frac{d^2\mathbf{q}}{(2\pi)^2} e^{i\mathbf{q} \cdot \mathbf{r}} (\hat{\mathbf{q}}_\perp)_\alpha (\hat{\mathbf{q}} + i\hat{\mathbf{d}})_\beta e^{-q d} \left[ \frac{1}{\hbar} G_0^R(\mathbf{q}, \omega) + \frac{e^2 \rho_e}{m} \right], \quad (50)$$

where we assumed  $d > 0$  and used the right-handed basis  $\hat{\mathbf{q}}_\perp, \hat{\mathbf{q}}, \hat{\mathbf{d}}$ . Next, we assume an isotropic response  $G_0^R(\mathbf{q}, \omega) = G_0^R(q, \omega)$ , and perform the integration over the azimuthal angle of  $\mathbf{q}$ . We arrive at

$$\chi_{\alpha\beta}(\rho, \varphi, \omega) = \frac{2\pi\gamma_e}{c} \int_0^{+\infty} \frac{q dq}{2\pi} K_{\alpha\beta}(q\rho, \varphi) e^{-q d} \left[ \frac{1}{\hbar} G_0^R(q, \omega) + \frac{e^2 \rho_e}{m} \right], \quad (51)$$

where we parametrize  $\mathbf{r}$  by polar coordinates  $\rho$  and  $\varphi$ . Here, we defined

$$K_{\alpha\beta}(q\rho, \varphi) = \begin{pmatrix} -\frac{1}{2} [J_0(q\rho) + J_2(q\rho)] \sin \varphi & \frac{1}{2} [J_0(q\rho) + J_2(q\rho)] \cos \varphi & 0 \\ -\frac{1}{2} [J_0(q\rho) - J_2(q\rho)] \cos \varphi & -\frac{1}{2} [J_0(q\rho) - J_2(q\rho)] \sin \varphi & J_1(q\rho) \end{pmatrix}_{\alpha\beta}, \quad (52)$$

where  $J_n$  are Bessel functions of the first kind and we take  $\alpha = \rho, \varphi, \beta = x, y, d$ .

### A. Current-current response

We calculate the current-current response  $G_0^R$  for the free Fermi gas with dispersion relation  $\omega_{\mathbf{k}} = \frac{\hbar \mathbf{k}^2}{2m}$  and at zero temperature:

$$\begin{aligned} G_0^R(\mathbf{q}, t) &= -i\Theta(t) \frac{1}{\mathcal{A}} \langle [J_\perp(\mathbf{q}, t), J_\perp(-\mathbf{q}, 0)] \rangle_0 \\ &= -i\Theta(t) \frac{1}{\mathcal{A}} \left( \frac{e\hbar}{m} \right)^2 \sum_{\sigma, \mathbf{k}} (\hat{\mathbf{q}}_\perp \cdot \mathbf{k})^2 \left\langle [\psi_{\sigma, \mathbf{k}}^\dagger(t) \psi_{\sigma, \mathbf{k}+\mathbf{q}}(t), \psi_{\sigma, \mathbf{k}+\mathbf{q}}^\dagger \psi_{\sigma, \mathbf{k}}] \right\rangle_0, \end{aligned} \quad (53)$$

where  $\mathcal{A}$  is the area of the 2D plane, and in the second step we inserted Eq. (10). Its Fourier components  $G_0^R(\mathbf{q}, \omega)$  can be calculated exactly in two dimensions:

$$G_0^R(q, \omega) = \frac{e^2 \rho_e}{m} \frac{2\hbar k_F}{3q} \left[ g\left(\frac{\omega}{v_F q} + \frac{q}{2k_F}\right) - g\left(\frac{\omega}{v_F q} - \frac{q}{2k_F}\right) \right], \quad (54)$$

where  $g(x)$  is a complex piecewise function:

$$\begin{aligned} \text{Re}[g(x)] &\equiv x^3 - \frac{3}{2}x - (x^2 - 1)^{\frac{3}{2}} \Theta(x^2 - 1) \text{sign}(x) \\ \text{Im}[g(x)] &\equiv (1 - x^2)^{\frac{3}{2}} \Theta(1 - x^2). \end{aligned} \quad (55)$$



It can be shown that the real and imaginary parts of  $g(x)$  satisfy the Kramers-Kronig relations. The Green's function simplifies under the assumption  $q \ll k_F$  to

$$G_0^R(q, \omega) \approx \frac{e^2 \rho_e}{m} \frac{2\hbar}{3} g' \left( \frac{\omega}{v_F q} \right), \quad (56)$$

where  $g'(x) = \partial_x g(x)$ .

We remark that the imaginary part of the current response  $\text{Im } G_0^R$  from Eq. (56) (capturing dissipation) and the magnetic noise  $C^{-+}$  from Eq. (20) (originating from current fluctuations) are related to each other via the fluctuation-dissipation theorem:

$$C^{-+}(\omega, q) = -\frac{8\pi^2}{c^2} e^{-2qd} \text{Im } G_0^R(\omega, q), \quad (57)$$

where we used Eq. (12).

## B. Dynamic response

The current response  $\mathbf{J}(\mathbf{r}, t)$  can be obtained by numerical integration of Eq. (49) and Eq. (51). The result is shown in Fig. ?? of the main text. We can see that  $\mathbf{J}$  travels away from the origin with velocity  $v_F$  and decays with some scaling.

To better understand these features, we find some approximation for  $\mathbf{J}^{\text{para}}$ . While the diamagnetic current can be calculated exactly as localized standing waves, the paramagnetic response can be fitted by a simple analytic expression for large  $\rho$  and  $\omega$ . In the end, we can show that:

$$\chi_{\alpha\beta}^{\text{para}}(\rho, \varphi, \omega) \approx \frac{2e^2 \rho_e \gamma_e}{mc} \frac{e^{i\frac{\omega}{v_F}\rho}}{\rho^2} \begin{pmatrix} \frac{iv_F}{\omega\rho} \sin \varphi & -\frac{iv_F}{\omega\rho} \cos \varphi & 0 \\ -\cos \varphi & -\sin \varphi & -i \text{sign}(\omega) \end{pmatrix}_{\alpha\beta}, \quad (58)$$

$$\chi_{\alpha\beta}^{\text{dia}}(\rho, \varphi) \approx -\frac{e^2 \rho_e \gamma_e}{mc} \frac{1}{\rho^2} \begin{pmatrix} \sin \varphi & -\cos \varphi & 0 \\ -\cos \varphi & -\sin \varphi & -1 \end{pmatrix}_{\alpha\beta}, \quad (59)$$

for  $\rho\omega/v_F \gg 1$  and  $d \rightarrow 0$ , where we have used the approximation from Eq. (56) for  $q \ll k_F$ . The validity of these approximations has been checked by numerical integration. Therefore, we expect that the paramagnetic current response  $\mathbf{J}^{\text{para}}$  follows the same scaling  $J_\rho^{\text{para}} \propto \rho^{-3}$  and  $J_\varphi^{\text{para}} \propto \rho^{-2}$  at long distance [9]. Also,  $\mathbf{J}^{\text{para}}$  should have the traveling-wave form because of the propagation factor  $e^{i\frac{\omega}{v_F}\rho}$  in the response function. Then we can parameterize  $\mathbf{J}^{\text{para}}$  as:

$$\begin{aligned} J_\rho^{\text{para}}(\rho, \varphi, t) &\sim \frac{1}{\rho^3} \left[ -h_{\rho x}^{\text{para}} \left( t - \frac{\rho}{v_F} \right) \sin \varphi + h_{\rho y}^{\text{para}} \left( t - \frac{\rho}{v_F} \right) \cos \varphi \right], \\ J_\varphi^{\text{para}}(\rho, \varphi, t) &\sim \frac{1}{\rho^2} \left[ -h_{\varphi x}^{\text{para}} \left( t - \frac{\rho}{v_F} \right) \cos \varphi - h_{\varphi y}^{\text{para}} \left( t - \frac{\rho}{v_F} \right) \sin \varphi + h_{\varphi d}^{\text{para}} \left( t - \frac{\rho}{v_F} \right) \right], \end{aligned} \quad (60)$$

where  $J_\rho^{\text{para}}$  and  $J_\varphi^{\text{para}}$  are the radial and azimuthal components of  $\mathbf{J}^{\text{para}}$ , and  $h_{\alpha\beta}^{\text{para}}$  are determined by both the response  $\chi_{\alpha\beta}^{\text{para}}$  and the spin dynamics  $\mathbf{S}(t)$ , with the oscillatory parts approximated as:

$$h_{\alpha\beta}(\xi) \sim \Theta(\xi) e^{-\frac{N}{2}\gamma_0\xi} \begin{pmatrix} -\frac{v_F}{\Delta} \sin(\Delta\xi) & \frac{v_F}{\Delta} \cos(\Delta\xi) & 0 \\ \cos(\Delta\xi) & \sin(\Delta\xi) & 0 \end{pmatrix}_{\alpha\beta} + \tilde{h}_{\alpha\beta}(\xi), \quad (61)$$

where  $\xi \equiv t - \rho/v_F$  and  $\tilde{h}_{\alpha\beta}$  are some non-oscillatory functions. Thus,  $\mathbf{J}^{\text{para}}$  captures the ballistic current wave. We can see that the paramagnetic current distribution forms the pattern of Archimedean spirals with two arms. These two spiral arms merge at the origin (the position of the macrospin) in a way that ensures  $\nabla \cdot \mathbf{J} = 0$ . In addition, the spirals are superimposed by loop currents that favor an overall clockwise current direction (in accordance with Lenz's law).

Finally, we note that, the total response current shown in Fig. 3 also contains the diamagnetic contribution  $\mathbf{J}^{\text{dia}}$  given in Eq. (47) whose dynamics is directly determined by the vector potential.

### C. Static response

Finally, we show that the static response agrees with the well known result of Landau diamagnetism. By relating the loop currents to a magnetization,  $m_J^d = \frac{i}{cq} \hat{\mathbf{d}} \cdot (\hat{\mathbf{q}} \times \langle \mathbf{J} \rangle)$ , and the vector potential to the magnetic field,  $H^d = -i\hat{\mathbf{d}} \cdot (\mathbf{q} \times \mathbf{A})$ , we find from Eq. (47) the magnetic response,  $m_J^d = \chi_{\text{Landau}} H^d$ . Hence, we determine the magnetic susceptibility as [10]

$$\chi_{\text{Landau}} = \lim_{\omega \rightarrow 0} \frac{-1}{c^2 q^2} \left( \frac{1}{\hbar} G_0^R(\mathbf{q}, \omega) + \frac{e^2 \rho_e}{m} \right) = -\frac{e^2}{12\pi m c^2} = -\frac{1}{3} \chi_{\text{Pauli}} \frac{m_e}{m}, \quad (62)$$

where we used Eq. (53). Here,  $m_e$  is the free electron mass, and  $m$  the effective band mass of the electron. In addition, we remark that the spatial dependence of the static response scales as  $\langle \mathbf{J} \rangle \propto \rho^{-4}$ , which follows from Eq. (51) for  $\omega \rightarrow 0$  and  $d \rightarrow 0$ . Hence, it decays much quicker than the dynamic response and is not resolved in Fig. 3 of the Letter.

- 
- [1] X. Li, J. Marino, D. E. Chang, and B. Flebus, [A solid-state platform for cooperative quantum dynamics driven by correlated emission](#) (2024), [arXiv:2309.08991 \[quant-ph\]](#).
  - [2] B. Flebus and Y. Tserkovnyak, Quantum-impurity relaxometry of magnetization dynamics, *Phys. Rev. Lett.* **121**, 187204 (2018).
  - [3] S. P. Kelly and Y. Tserkovnyak, [Superconductivity-enhanced magnetic field noise](#) (2024), [arXiv:2412.05465 \[cond-mat.supr-con\]](#).
  - [4] R. H. Dicke, Coherence in spontaneous radiation processes, *Phys. Rev.* **93**, 99 (1954).
  - [5] W.-K. Mok, A. Poddar, E. Sierra, C. C. Rusconi, J. Preskill, and A. Asenjo-Garcia, [Universal scaling laws for correlated decay of many-body quantum systems](#) (2024), [arXiv:2406.00722 \[quant-ph\]](#).
  - [6] S. J. Masson and A. Asenjo-Garcia, Universality of dicke superradiance in arrays of quantum emitters, *Nature Communications* **13**, 2285 (2022).
  - [7] Supplemental material (2024), see Supplemental Material for video of current emission.
  - [8] P. Coleman, *Introduction to Many-Body Physics* (Cambridge University Press, 2015).
  - [9] For small distance, we need different approximation to capture the low frequency response, and the scaling is also not correct in that regime.
  - [10] H. B. Singh and K. N. Pathak, Diamagnetic susceptibility of an interacting electron gas, *Phys. Rev. B* **11**, 4246 (1975).